MNRAS **456,** 2647–2653 (2016) doi:10.1093/mnras/stv2695

SAX J1808.4−3658, an accreting millisecond pulsar shining in gamma rays?

E. de Oña Wilhelmi,[1⋆] A. Papitto,[1⋆] J. Li,[1] N. Rea,[1,2] D. F. Torres,[1,3] L. Burderi,[4] T. Di Salvo,[5] R. Iaria,[5] A. Riggio[4] and A. Sanna[4]

[1]*Institute for Space Sciences (CSIC−IEEC), Campus UAB, Carrer de Can Magrans s/n, 08193 Barcelona, Spain*
[2]*Anton Pannekoek Institute for Astronomy, University of Amsterdam, Postbus 94249, NL-1090 GE Amsterdam, the Netherlands*
[3]*Institució Catalana de Recerca i Estudis Avançats (ICREA), 08010 Barcelona, Spain*
[4]*Università degli Studi di Cagliari, Dipartimento di Fisica, SP Monserrato-Sestu, KM 0.7, 09042 Monserrato, Italy*
[5]*Dipartimento di Fisica e Chimica, Università di Palermo, via Archirafi 36, 90123 Palermo, Italy*

Accepted 2015 November 16. Received 2015 November 13; in original form 2015 June 3

ABSTRACT

We report the detection of a possible gamma-ray counterpart of the accreting millisecond pulsar SAX J1808.4−3658. The analysis of ∼6 yr of data from the Large Area Telescope on board the *Fermi* gamma-ray Space Telescope (*Fermi*-LAT) within a region of 15° radius around the position of the pulsar reveals a point gamma-ray source detected at a significance of $\sim 6\sigma$ (test statistic TS = 32), with a position compatible with that of SAX J1808.4−3658 within the 95 per cent confidence level. The energy flux in the energy range between 0.6 and 10 GeV amounts to $(2.1 \pm 0.5) \times 10^{-12}$ erg cm^{-2} s^{-1} and the spectrum is represented well by a power-law function with photon index 2.1 ± 0.1. We searched for significant variation of the flux at the spin frequency of the pulsar and for orbital modulation, taking into account the trials due to the uncertainties in the position, the orbital motion of the pulsar and the intrinsic evolution of the pulsar spin. No significant deviation from a constant flux at any time-scale was found, preventing a firm identification via time variability. Nonetheless, the association of the LAT source as the gamma-ray counterpart of SAX J1808.4−3658 would match the emission expected from the millisecond pulsar, if it switches on as a rotation-powered source during X-ray quiescence.

Key words: stars: individual: SAX J1808.4-3658 – stars: neutron – gamma-rays: stars.

1 INTRODUCTION

Accretion-powered millisecond pulsars (AMSPs) are neutron stars (NSs) that orbit a low-mass companion star ($\lesssim 1$ M$_\odot$) and show coherent X-ray pulsations at periods of a few milliseconds during X-ray flares known as outbursts, caused by the impact of an accretion stream on to the NS surface. The coherent pulsations observed in the X-ray light curve during outbursts are due to the channelling by the NS magnetosphere of (at least part of) the accretion flow to the magnetic poles of the NS.

SAX J1808.4−3658 was the first AMSP discovered (Wijnands & van der Klis 1998); since 1996, it has gone into an outburst a few weeks long eight times, i.e. roughly every 2.5 yr (Patruno & Watts 2012 and references therein, and Sanna et al. 2015 for the most recent one) reaching a peak X-ray luminosity of a few times 10^{36} erg s^{-1}. During X-ray quiescence, it shows a much fainter unpulsed X-ray emission, which attains a 0.5–10 keV luminosity ranging between 0.5 and 1×10^{32} erg s^{-1} (Campana et al. 2002; Heinke et al. 2007).

Millisecond pulsars (MSPs) are believed to achieve their fast rotation during a gigayear-long phase of accretion of mass and angular momentum from a companion star (Alpar et al. 1982; Radhakrishnan & Srinivasan 1982). When the mass-transfer rate declines at the end of the accretion phase, the NS magnetosphere is able to expand up to the light cylinder, and the pulsar switches on as an MSP powered by the rotation of its magnetic field. MSPs accelerate electron/positron pairs along field lines, driving a pulsed emission observed mainly in the radio and gamma-ray bands. The close link between accreting NSs and MSPs was recently demonstrated by the discovery of IGR J18245−2452, which during an outburst was observed as an AMSP, after having been previously detected as a radio MSP during X-ray quiescence (Papitto et al. 2013). This source switches between these two states over a few weeks, presumably

⋆E-mail: wilhelmi@ieec.uab.es (MW); papitto@ice.csic.es (AP)

in response to variations of the mass inflow rate (Stella et al. 1994; Campana et al. 2002; Burderi et al. 2003). Several indirect indications have been collected that a radio pulsar turns on during the quiescent state of other AMSPs. For SAX J1808.4−3658, in particular, the amount of optical light reprocessed by the companion star during X-ray quiescence (Homer et al. 2001) is compatible with irradiation by a radio pulsar (Burderi et al. 2009), the decrease of the NS spin period between consecutive outbursts is similar to the rate observed for MSPs (Hartman et al. 2009; Patruno et al. 2012), and the rapid increase of the orbital period suggests ejection of the mass transferred from the companion star and/or changes in the mass quadrupole moment of the companion (di Salvo et al. 2008; Burderi et al. 2009; Patruno et al. 2012). However, radio pulsations have not been detected from either SAX J1808.4−3658 or other AMSPs (Burgay et al. 2003; Iacolina et al. 2009, 2010), except for IGR J18245-2453 (Papitto et al. 2013). This could be due to an intrinsic low luminosity of the radio pulsar, geometrical effects, and/or free–free absorption from material ejected from the system by the pulsar radiation pressure (di Salvo et al. 2008). Note that two more MSPs, PSR J1023+0038 (Archibald et al. 2009; Patruno et al. 2014) and XSS J12270-4859 (Bassa et al. 2014), have been observed in an intermediate state characterized by the presence of an outer accretion disc, and during which accretion-powered X-ray pulsations were detected (Archibald et al. 2014; Papitto et al. 2015). However, the X-ray luminosity of these sources during such episodes ($\approx 5 \times 10^{33}$ erg s^{-1}) is much fainter than that usually attained by AMSPs, which possibly indicates that a large fraction of the mass inflow is ejected by the quickly rotating NS magnetosphere rather than accreted on to the NS surface.

Turning to high energies (100 MeV $< E <$ 100 GeV) is a promising strategy for detecting the emission expected from an MSP turned on during the X-ray quiescent state of an AMSP. The Large Area Telescope on the *Fermi* gamma-ray Space Telescope (*Fermi*-LAT; Atwood et al. 2009) has proved to be an efficient rotation-powered MSP detector (Abdo et al. 2013), benefiting from the larger emission angle in gamma rays, and the absence of absorption from material possibly enshrouding the binary. The gamma-ray pulsar sample comprises not only canonical young pulsars but also recycled MSPs, which generally show a similar spectral shape as the young ones. The sky region of several AMSPs was investigated by Xing & Wang (2013) in a search for gamma-ray emission in the 100 MeV to 300 GeV range over 4 yr, but they did not detect significant emission associated with any AMSP. A source compatible with the position of SAX J1808.4−3658 and dubbed 3FGL J1808.4−3703, is listed in the recently published *Fermi*-LAT 4-yr point source catalogue (3FGL, Acero et al. 2015) with a detection significance of 4.5σ. Also, a possible detection of the gamma-ray counterpart of SAX J1808.4−3658 was reported by Xing, Wang & Jithesh (2015), who nevertheless searched for gamma-ray pulsations using only the nominal values of the ephemeris reported in Hartman et al. (2009), apparently overlooking the effect of the uncertainties of the position and orbital and spin parameters over the coherence of a signal searched in a time series a few years long. Here we analyse almost 6 yr of LAT data from the region around SAX J1808.4−3658 to investigate the possibility of the source emitting a significant fraction of its energy in the gamma-ray regime. We performed a detailed timing analysis to search for periodic features that could firmly identify the gamma-ray source as the counterpart of SAX J1808.4−3658, carefully treating the impact of the uncertainties of the system timing and spatial parameters on the range of parameters that have to be considered.

2 DATA ANALYSIS AND RESULTS

2.1 Data analysis

To search for a gamma-ray counterpart of SAX J1808.4−3658, we analysed data obtained with *Fermi*-LAT in a region of 15° radius around its position ($\mathrm{RA_{J2000}} = 18^{\mathrm{h}}08^{\mathrm{m}}27\overset{\mathrm{s}}{.}62$, $\mathrm{Dec_{J2000}} = -36°58'43\overset{''}{.}3$, Hartman et al. 2008). The LAT experiment on board the *Fermi Gamma-ray Space Telescope* satellite is sensitive to gamma rays with energies from 20 MeV to above 300 GeV, recording events with a timing accuracy better than 1 μs (Abdo et al. 2009). Almost 6 yr of data (`P7REP`, SOURCE class) obtained between the beginning of the operation MJD 54 682.6 (2008 August 4) and MJD 56 812.4 (2014 June 4) were processed using the publicly available *Fermi*-LAT Science Tools (software version v9r32p5), analysed with the response functions `P7REP_SOURCE_V15` and using the templates for Galactic (gll_iem_v05.fits) and isotropic (iso_source_v05.txt) backgrounds. We selected data in the 100 MeV to 300 GeV energy range. Standard time event cuts performed with the tool `gtmktime` (`DATA_QUAL==1`, `LAT_CONFIG==1` and `ABS(ROCK_ANGLE)<52`) were applied. To suppress the effect of the Earth limb background, we excluded time intervals when the Earth was in the field of view (when the LAT Z-axis was more than 52° from the zenith), and those in which part of the selected region of interest was observed with zenith angle larger than 100°. A second analysis was performed excluding the periods in which SAX J1808.4−3658 was in an X-ray bright outburst state, i.e. between 2008 September 22 and November 7 and 2011 November 5 to 20 (Hartman et al. 2009; Patruno et al. 2012), with compatible results to those presented next. No significant gamma-ray excess is detected when analysing time intervals when the source was in outburst.

2.2 Image and spectral analysis

The image of the sky around the position of SAX J1808.4−3658 was obtained in the energy range above 1 GeV, where the angular resolution of *Fermi*-LAT reaches ≈0.8°[1] on axis. Using the same exposure and instrument response from the data set, we modelled the region of interest with all the 3FGL sources (Acero et al. 2015) (excluding 3FGL J1808.4−3703) and the standard Galactic and isotropic diffuse components and we left all the spectral parameters to be free (except for the spectra of the sources more than 10° away from the centre) in a maximum likelihood fit (using `gtlike`[2]). Fig. 1 shows the residuals with respect to the best-fitting model. The residual image shows a point source compatible with the position of SAX J1808.4−3658 (see blue cross). For the computation of the significance and spectral parameters of SAX J1808.4−3658, we added a point source at $\mathrm{RA_{J2000}} = 272.115°$ and $\mathrm{Dec_{J2000}} = -36.98°$ to account for the gamma-ray excess.

The inclusion of a point gamma-ray source at the position of SAX J1808.4−3658 described with a power-law function, $\phi_0 \times (E/E_0)^{-\Gamma}$, normalized at $E_0 = 1.44$ GeV with $\phi_0 = (2.42 \pm 0.56) \times 10^{-10}$ GeV^{-1} cm^{-2} s^{-1} and $\Gamma = 2.1 \pm 0.1$ (in black in Fig. 2), results in a test statistic (Mattox et al. 1996) value of 31.6, which corresponds to a source detection at a confidence level (CL) of $\sim 6\sigma$. Applying the *pointlike maximum-likelihood fitting* package (Kerr 2010), we fit the position of the gamma-ray excess above 100 MeV to $\mathrm{RA_{J2000}} = (272.143 \pm 0.037)°$ and

[1] http://www.slac.stanford.edu/exp/glast/groups/canda/lat_Performance.htm
[2] http://fermi.gsfc.nasa.gov/ssc/data/analysis/scitools/

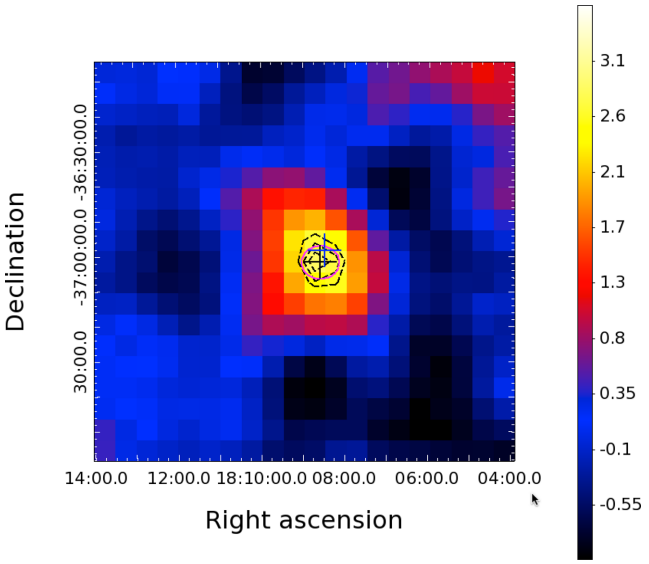

Figure 1. *Fermi*-LAT residual $2 \times 2^\circ$ (using a pixel size of $0.1 \times 0.1^\circ$) count map above 1 GeV of the SAX J1808.4−3658 region smoothed with a Gaussian of width $\sigma = 0.3^\circ$ (units of the scale on the right are counts). The best-fitting position of the gamma-ray source is marked with a black cross whereas the position of SAX J1808.4−3658 is marked in blue. The black-dashed lines show the test statistic significance contours above 1 GeV corresponding to CLs of 68 per cent, 95 per cent and 99 per cent. The magenta circle shows the 95 per cent CL error in the best-fitting position.

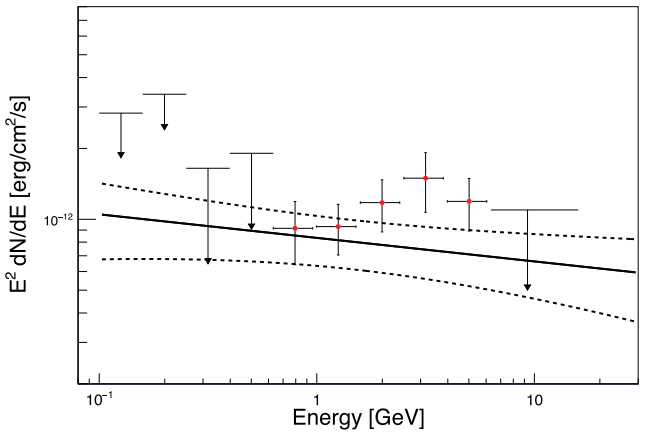

Figure 2. Spectral energy distribution obtained at the position of SAX J1808.4−3658. The best-fitting power law function is plotted as a solid line, and the dashed lines show the statistical errors in the global fit. No highly significant improvement (by less than 3σ) is obtained using more sophisticated models, such as a power law with a cut-off at high energies function or a log parabola function. The best-fitting functions for the latter models are shown in dash-dot-dot and dash-dot lines for exponential cut-off and log parabola functions, respectively.

$\mathrm{Dec_{J2000}} = (-37.034 \pm 0.032)^\circ$ (compatible with the position of SAX J1808.4−3658 within 95 per cent CL, see magenta circle in Fig. 1). The contour lines for the 68, 95 and 99 per cent CLs obtained from the significance map, calculated with `gttsmap` for events above 1 GeV, are also shown.

The spectral energy distribution for a point source centred on the position of SAX J1808.4−3658 was derived by means of a binned likelihood fitting, divided into 15 logarithmic bins between 100 MeV and 300 GeV (see Fig. 2). The spectral points obtained for each energy bin (with significance of more than 2σ), fitting the data with a power-law function with fixed photon index of 2, are shown in Fig. 2. More sophisticated spectral shapes, aiming to fit the 100 MeV to 300 GeV spectral range, do not provide a statistically significant improvement to the fit. The comparison with a fit to a log parabola function [$\phi = \phi_0 (E/E_\mathrm{b})^{-(\alpha+\beta \log(E/E_\mathrm{b}))}$] results in a difference in the maximum likelihood of $2 \times \Delta L/\Delta$[Number of Degrees of Freedom (ndf)] = 10 [with Δ(ndf) = 2 and probability $P = 6.7 \times 10^{-3}$, corresponding to 2.7σ], whereas the comparison to a power-law function plus exponential cut-off [$\phi = \phi_0 (E/E_0)^{-\gamma_1} \exp(-(E/E_\mathrm{c}))$] leads to an increase of only 8 [with Δ(ndf) = 1 and probability $P = 4.57 \times 10^{-3}$, corresponding to 2.8σ]. For the log parabola hypothesis, the best-fitting parameters we found are $\phi_0 = (4.20 \pm 0.32) \times 10^{-10}\,\mathrm{GeV^{-1}\,cm^{-2}\,s^{-1}}$, $\alpha = 1.91 \pm 0.09$ and $\beta = 0.41 \pm 0.02$ for a break energy of $E_\mathrm{b} = 1.4$ GeV, whereas when we try to fit to a power-law function plus exponential cut-off, we obtain $\phi_0 = (3.2 \pm 2.7) \times 10^{-8}\,\mathrm{GeV^{-1}\,cm^{-2}\,s^{-1}}$, $\gamma = 1.4 \pm 0.4$ and $E_\mathrm{c} = 3.8 \pm 25$ GeV.

2.3 Timing analysis

The long-term exposure-corrected (counts/exposure) light curve, produced by *aperture photometry* within a radius of 1° and retaining photons between 100 MeV and 300 GeV, does not show any deviation from a constant flux. The fit to a constant flux results in a χ^2/ndf of 0.9 (for ndf = 210) using a linear binning with a bin width of 10 d. To search for a modulation of the gamma-ray flux at the orbital period of the gamma-ray flux, we folded the light curve in 10 bins around the value of the orbital period predicted according to

$$P_\mathrm{orb}(t) = P_\mathrm{orb}(T_0) + \dot{P}_\mathrm{orb}(T_0) \times (t - T_0) + \frac{1}{2} \ddot{P}_\mathrm{orb}(T_0) \times (t - T_0)^2, \quad (1)$$

where $T_0 = 54\,730$ MJD, and the values of $P_\mathrm{orb}(T_0)$, $\dot{P}_\mathrm{orb}(T_0)$ and $\ddot{P}_\mathrm{orb}(T_0)$ are listed in Table 1 (di Salvo et al. 2008; Burderi et al. 2009; Patruno et al. 2012). The variance of the folded profile extracted considering photons at energies larger than 100 MeV is χ^2/ndf = 11/9, indicating no evidence of a significant modulation. A similar result is obtained considering only photons at higher energies (e.g. >2 GeV). The fit to a constant function results in a χ^2/ndf of 30/9 (see Fig. 3), corresponding to a marginal P value of 5×10^{-4} pre-trial.

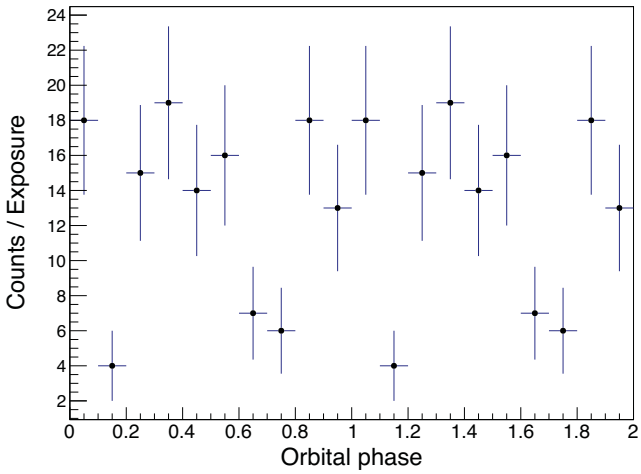

Figure 3. Phaseogram obtained by folding the arrival time of the exposure-corrected gamma-ray photons $E > 2$ GeV with the orbital period $P_\mathrm{orb}(t)$ obtained from equation (1).

Table 1. Parameters used in the periodicity search.

Parameter	Best estimate, x_i	Error, σ_{x_i}	Sensitivity, δ_{x_i}	Number of corrections, N_{x_i}
Ecliptic longitude, λ	271.737 918°	0.13 arcsec	0.015 arcsec	16
Ecliptic latitude, β	−13.552 162°	0.15 arcsec	0.064 arcsec	5
Orbital period, $P_{\rm orb}(T_0)$	7249.157 964 s	7.6×10^{-5} s	3.4×10^{-4} s	1
Orbital period derivative, $\dot{P}_{\rm orb}(T_0)$	3.17×10^{-12}	0.70×10^{-12}	1.8×10^{-12}	1
Orbital period second derivative, $\ddot{P}_{\rm orb}(T_0)$	1.65×10^{-20} s^{-1}	0.35×10^{-20} s^{-1}	2.0×10^{-20} s^{-1}	1
Epoch of passage at ascending node, T^*	54 729.999 079 MJD	0.78 s	14.9 s	1
Semi-major projected axis, $a \sin i/c$	62.812 light-milliseconds	2×10^{-3} light-milliseconds	2.0 light-milliseconds	1
Spin frequency, $\nu(T_0)$	400.975 210 14 Hz	2.4×10^{-2} μHz	5.4×10^{-3} μHz	27
Spin frequency derivative, $\dot{\nu}$	7.1×10^{-16} Hz s^{-1}	-1.2×10^{-16} Hz s^{-1}	3.3×10^{-17} Hz s^{-1}	25

Notes. Position and orbital parameters were taken from Hartman et al. (2008, 2009) and Patruno et al. (2012). Frequency and the frequency derivative were measured by fitting the spin frequency values given by Hartman et al. (2008, 2009) and Patruno et al. (2012) with a constant spin-down function (see black dashed line in Fig. 4). The reference epoch is $T_0 =$ MJD 54 730. The total observation time is $T_{\rm obs} = 2129.8$ d. See Section 2.2 for details of the assessment of the sensitivity to a coherent signal over the considered time series.

The search for gamma-ray pulsations is limited by the uncertainties in the ephemeris and position of the source and the (faint) flux level detected. This search must take into account the loss of signal coherency over the $T_{\rm obs} = 2129.8$-d interval spanned by the observations. The following effects are considered: (i) the orbital motion of the pulsar, (ii) the intrinsic evolution of the pulsar spin and (iii) uncertainties in the position of the source.

The frequency variations induced by the orbital motion of the source have to be taken into account by correcting the photon arrival times to the line of nodes of the binary system, using the most updated orbital solution available (see Table 1). Assuming that the orbital period evolution is described by equation (1), the maximum uncertainty on the estimate of the orbital period driven by the errors on the values of $P_{\rm orb}(T_0)$, $\dot{P}_{\rm orb}(T_0)$ and $\ddot{P}_{\rm orb}$, is evaluated by standard error propagation over the length of the considered time series:

$$\sigma_{P_{\rm orb}}^{\rm max} = \left[\sigma_{P_{\rm orb}}^2 + (\sigma_{\dot{P}_{\rm orb}} T_{\rm obs})^2 + \left(\frac{1}{2}\sigma_{\ddot{P}_{\rm orb}} {T_{\rm obs}}^2\right)^2\right]^{1/2} = 1.6 \times 10^{-4}\ {\rm s}. \quad (2)$$

To check if the actual uncertainties of the orbital parameters produce a loss of coherence of the pulsar signal, we used the expressions given by Caliandro, Torres & Rea (2012, see table 3 therein), who estimated the fraction of power lost, ϵ, as a function of the difference between the actual value of an orbital parameter and the one used to refer photon times of arrival to the line of nodes of the binary system. We evaluated the analytical relations they give for a circular orbit,

$$\delta(a \sin i/c) = \frac{1}{2\nu_0}\frac{1}{\epsilon^2}, \quad (3)$$

$$\delta T^* = \frac{0.1025 P_{\rm orb}}{\pi \nu_0 (a \sin i/c)}\frac{1}{\epsilon^2} \quad (4)$$

and

$$\delta P_{\rm orb} = \frac{{P_{\rm orb}}^2}{2\pi\nu_0 (a \sin i/c) T_{\rm obs}}\sqrt{\left(\frac{1-\epsilon^2}{10}\right)}, \quad (5)$$

for $\epsilon = 0.8$, obtaining the values listed in Table 1 in the column labelled as 'Sensitivity'. Here, $a \sin i/c$ is the projected semi-major axis of the NS orbit, and T^* is the epoch of passage of the NS at the ascending node of the orbit. For each of the orbital parameters, x_i, the sensitivity value δ_{x_i} is larger than the uncertainty σ_{x_i} (see Table 1), which ensures that signal coherence is not lost throughout the length of the considered observation. The sensitivities to the uncertainty of the first and second derivatives of the orbital period were evaluated by taking the value that alone would produce a period shift equal to $\delta P_{\rm orb}$, namely, $\delta \dot{P}_{\rm orb} = \delta P_{\rm orb}/T_{\rm obs}$ and $\delta \ddot{P}_{\rm orb} = 2\delta P_{\rm orb}/T_{\rm obs}^2$ (see equation 1).

So far, coherent pulsations have been detected from SAX J1808.4−3658 only in the X-ray light curves observed during six of the outbursts shown by the source since 1998, each of which lasted a few weeks. We extrapolated the spin evolution of the pulsar, fitting a constant spin-down model to the frequencies measured in different outbursts. In addition, the measure of the spin frequency of SAX J1808.4−3658 during each of the outbursts is complicated by the presence of strong timing noise that exceeds Poisson counting noise and affects, to a different extent, the first and second harmonics of the signal (Burderi et al. 2009). Hartman et al. (2009) and Patruno et al. (2012) measured the frequency of the signal during each of the outbursts using a frequency-domain filter to weigh the harmonics according to the observed noise properties and estimated the uncertainty by performing Monte Carlo simulations. Using this method, they found no significant evolution of the spin frequency during the various outbursts. Here we consider the spin frequency that they measured in each of the outbursts, summing in quadrature the uncertainty driven by positional errors $\delta\nu_{\rm pos}^{\rm max}$ (see below) to the uncertainty quoted for their values. By fitting the average frequency values observed during the six different outbursts with a constant spin-down trend,

$$\nu(t) = \nu(T_0) + \dot{\nu} \times (t - T_0), \quad (6)$$

we estimated the spin frequency derivative as $\dot{\nu} = (7.1 \pm 1.2) \times 10^{-16}$ Hz s^{-1} (see dashed line in Fig. 4), compatible with the value given by Patruno et al. (2012). Propagating the errors for the spin frequency and its derivative over the whole length of the observations leads to a maximum uncertainty of the signal frequency of

$$\sigma_\nu^{\rm max} = [\sigma_\nu^2 + (\sigma_{\dot{\nu}} T_{\rm obs})^2]^{1/2} \simeq 3 \times 10^{-2}\ \mu{\rm Hz}. \quad (7)$$

We assume that the minimum difference between frequencies that produces a significant power loss in a search for a signal is equal to the independent Fourier frequency spacing, $\Delta\nu_{\rm IFS} = 1/T_{\rm obs} = 5.4 \times 10^{-3}$ μHz. As the maximum uncertainty of the spin frequency $\sigma_\nu^{\rm max}$ is larger than $\Delta\nu_{\rm IFS}$, we are forced to perform a search over different possible values of $\nu(T_0)$ and $\dot{\nu}$ to avoid a significant loss of signal power. We varied the spin frequency and its derivative in steps equal to the amount that produces an uncertainty equal to $\Delta\nu_{\rm IFS}$ over a time interval equal to

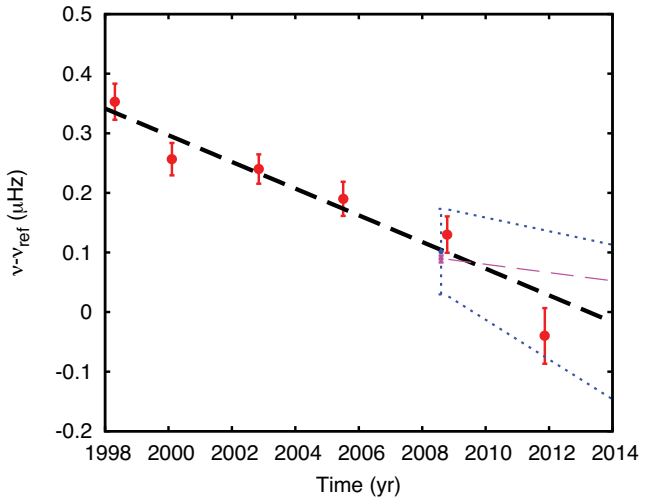

Figure 4. Evolution of the spin frequency of SAX J1808.4−3658 as observed in the X-ray band. The dashed black line is the best-fitting spin-down trend, the dotted blue lines mark the range of parameters searched, and the magenta line is the solution that gives the maximum H-test value. The reference frequency is $\nu_o = 400.975\,210$ Hz.

$T_{\rm obs}$, i.e. $\delta\nu = \Delta\nu_{\rm IFS} = 5.4 \times 10^{-3}$ μHz, and $\delta\dot{\nu} = \Delta\nu_{\rm IFS}/T_{\rm obs} = 1/T_{\rm obs}^2 = 2.9 \times 10^{-17}$ Hz s^{-1}. To cover an interval equal to $\pm 3\sigma$ around the central value of $\nu(T_0)$ and $\dot{\nu}$, we then performed $N_\nu = 2 \times (3\sigma_\nu)/\delta\nu = 27$ and $N_{\dot{\nu}} = 2 \times (3\sigma_{\dot{\nu}})/\delta\dot{\nu} = 25$ correction trials on the spin frequency and its derivative, respectively. The limits of the range of values covered are plotted in Fig. 4 using blue dashed lines.

An additional number of correction trials have to be performed when photon arrival times are converted to the Solar system barycentre, because of the uncertainty of the source position. We considered the position of the optical counterpart determined by Hartman et al. (2009), RA = $18^{\rm h}08^{\rm m}27\overset{\rm s}{.}62$, Dec = $-36^\circ 58' 43\overset{''}{.}3$, with an uncertainty of $0.15''$ [corresponding to ecliptic coordinates $\lambda = 271.737918^\circ$, $\beta = -13.552\,162^\circ$, affected by uncertainties $\sigma_\lambda = 013$ arcsec, and $\sigma_\beta = 0.15$ arcsec, respectively (see Table 1)]. A difference of $(\delta\lambda, \delta\beta)$ between the actual ecliptic coordinates of the source (λ, β), and those used to correct the time series, yields an apparent modulation of the spin frequency of the signal equal to:

$$\delta\nu_{\rm pos} = \nu y \left(\frac{2\pi}{P_\oplus}\right) [\cos A_0 \cos\beta\,\delta\lambda + \sin A_0 \sin\beta\,\delta\beta] \qquad (8)$$

(Manchester & Peters 1972). Here y is the distance of the Earth from the Solar system barycentre, $P_\oplus = 1$ yr, $A_0 = [2\pi(T_0 - T_\gamma)/P_\oplus]$, T_0 is the start time of observations and T_γ is the vernal point. Considering that our time series covers $\simeq$5.8 yr, the uncertainty on the position of SAX J1808.4−3658 translates into a modulation of the signal frequency of amplitude $\delta\nu_{\rm pos}^{\rm max} \simeq 2.4 \times 10^{-2}$ μHz. As for the uncertainty of the spin frequency and its derivative (see above), this value is also larger than the spacing between independent Fourier frequencies, $\Delta\nu_{\rm IFS} = 5.4 \times 10^{-3}$ μHz, forcing us to perform a series of corrections on the coordinates used to barycentre the *Fermi*-LAT light curve. We estimated the minimum difference between coordinates that produces a significant signal loss as that producing a frequency oscillation $\delta\nu_{\rm pos}$ (evaluated using equation 8 and putting $\cos A_0$ and $\sin A_0$ equal to one, for simplicity) equal to $\Delta\nu_{\rm IFS}$. We thus obtained $\delta\lambda = 0.015$ arcsec and $\delta\beta = 0.064$ arcsec. To cover a range within 1σ from the central estimates of the source coordinates, $N_\lambda = 2\sigma_\lambda/\delta_\lambda = 16$ and $N_\beta = 2\sigma_\beta/\delta_\beta = 5$ preliminary corrections of the time series were then performed (see Table 1, where the parameters of the grid used in the periodicity search are given). That implies $N_\lambda N_\beta = 80$ time series, for which $N_\nu N_{\dot{\nu}} = 675$ searches over ν and $\dot{\nu}$ should be performed. Considering the flux level of the detected source (with ∼100 photons detected from the source direction), the total number of trials needed to be applied ($N_{tr} = 54\,000$) strongly hampers the search for gamma-ray pulsations at the spin period of the source, given the current uncertainties and instrument sensitivity. Considering these values, only a signal with a sinusoidal amplitude $\gtrsim$65 per cent (i.e. giving $\chi^2/({\rm ndf}-1) = 5.75$ for ndf = 10) would be detected at 3σ CL by an epoch folding search technique, performed by sampling the profile with ndf = 10 phase bins (Leahy 1987).[3]

Nevertheless, we searched for a periodic signal in the *Fermi*-LAT light curve in the range considered in Fig. 4. The arrival time of each event was first transformed to the Solar system barycentre using the grid of positions determined previously, then we applied the corrections for the orbital motion, and finally we calculated the phase of each photon using the grid of values of frequency and frequency derivative determined above. The time correction was done using the LAT `gtpphase` tool. The uniformity of the phaseogram is tested by applying both a simple epoch folding search test on a 10-bin pulse profile and an H-test (de Jager & Büsching 2010) on the arrival events. Fig. 5(a) shows the distribution of the χ^2 obtained with an epoch folding search for different positions, ν and $\dot{\nu}$. The two tests reached a maximum $\chi^2/{\rm ndf} = 3.8$ (with ndf = 9) and $H = 11.7$ for $m = 2$, where m is the number of harmonics used when the data set is folded using the combination $\lambda_0 = 271.737\,942^\circ$, $\beta_0 = -13.552\,197^\circ$, $\nu_0 = 400.975\,210\,089$ Hz and $\dot{\nu}_0 = -2.2 \times 10^{-16}$ Hz s^{-1}. We performed the same statistics test around *fake* values of ν and $\dot{\nu}$ ($\nu_{\rm fake} = 399.975\,210\,13$ Hz and $\dot{\nu}_{\rm fake} = -5.5 \times 10^{-16}$ Hz s^{-1}) to validate the uniformity of the test (in red in Fig. 5a). de Jager & Büsching (2010) showed that the probability distribution for the H-test can be described by $P(>H) = \exp(-0.4H)$. From this expression, we can derive a probability $P(>11.7) = 9.3 \times 10^{-3}$ before trials for the light curve deviate from a flat distribution. The folded light curve obtained with ν_0 and $\dot{\nu}_0$ and the position (λ_0,β_0) is shown in Fig. 5(b) (two cycles are plotted for clarity), and the relevant source spin evolution is plotted as a magenta dashed line in Fig. 4. Also considering the large number of trials made ($N_{\rm tr} = 54\,000$), such a solution is not significant. Similarly, the probability of obtaining a chi-squared value of $\chi^2/{\rm ndf} = 3.8$ for ndf = 9 in a single epoch folding is $P = 8.2 \times 10^{-5}$. Considering all the trials made, we expect $N_{\rm tr} \times P \simeq 4.4$ folded profiles to yield such a chi-squared value by chance, which indicates clearly that the detection is not significant.

3 DISCUSSION

The best-fitting position of the gamma-ray source discovered is located 3.2 arcmin from the optical position of SAX J1808.4−3658 (within the 95 per cent CL of the gamma-ray source position). We investigated a region of 0.15° radius surrounding the position of the gamma-ray source, and no obvious possible gamma-ray-producing counterpart or gamma-ray accelerator was found beside the AMSP. The only source detected in the surroundings is the radio galaxy NVSS 180824−365813 (Condon et al. 1998), although the lack

[3] We note that the sensitivity to a signal with a lower duty cycle, like those often observed from radio pulsars, would be higher than for a sinusoidal signal.

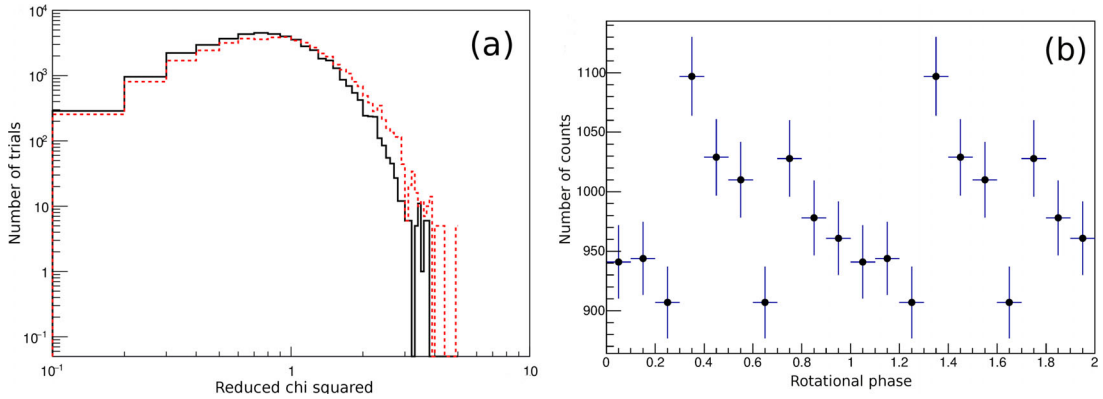

Figure 5. (a) χ^2/ndf distribution for positions, independent frequencies and frequency derivatives tested in a range of 3σ around the expected ν and $\dot{\nu}$ and of 1σ around the central estimate of the coordinates. The black distribution shows the results when using the correct ephemeris whereas the red one refers to the *fake* ones. (b) Phaseogram obtained by folding the arrival time of the gamma-ray photons with ν_0 and $\dot{\nu}_0$ and on the position λ_0 and β_0, which results in a maximum in the two periodicity tests applied. Two cycles are plotted for clarity, and the y-axis is zero-suppressed.

of an X-ray counterpart and faint flux make it an unlikely candidate to emit in gamma rays (Beckmann, Soldi & De Jong 2014). A more detailed investigation of faint X-ray sources other than SAX J1808.4−3658 can be found in Xing et al. (2015).

In the 3FGL catalogue, a source compatible with the position of SAX J1808.4−3658 and dubbed 3FGL J1808.4−3703 is listed. Its flux and spectral parameters are compatible with the source reported here. Xing et al. (2015) reported similar investigations. Nevertheless, a search for gamma-ray pulsations was done by the previous authors without taking into account the possible range of possible ephemerides. Xing et al. (2015) also reported a barely significant modulation at the orbital period. Here, a detailed timing analysis is performed, considering the uncertainties of the system timing and spacial parameters. We also checked that their result could be reproduced (with a statistical significance in the 10-bin light-curve of $\chi^2/\mathrm{ndf} = 30/9$, corresponding to 3.5σ) by extracting only photons with energies >2 GeV from a region around 0.6° around the source. The non-detection of any significant modulation when considering a region of different size or a different energy band raises doubts on the reliability of such a claim.

If the identification of the gamma-ray source found with the AMSP is real, the gamma-ray emission could originate either in the pulsar magnetosphere or in the intra-binary shock. No significant variation at the time-scale set by the orbital period has been found. We also folded the arrival times of the gamma-ray photons around the spin frequency of the pulsar, using the latest ephemeris measured during the last flaring state, and allowing a deviation of 3σ with respect to the extrapolated values for ν and $\dot{\nu}$. The position of the source was also varied to take into account the error in the position determination when converting to the Solar system barycentre. Considering the large number of trials needed to cover all the possible spin and position parameters, no significant detection of gamma-ray pulsations could be achieved. Even though we cannot yet formally identify the LAT source with SAX J1808.4−3658, we can compute the gamma-ray luminosity for a scenario in which SAX J1808.4−3658 is producing the detected gamma-ray radiation at a distance of 3.5 ± 0.1 kpc (Galloway & Cumming 2006). We obtain a total luminosity of $L_\gamma = (3 \pm 1) \times 10^{33}\,\mathrm{erg\,s^{-1}}$ in the energy range between 0.6 and 10 GeV (i.e. the energy range in which the source was significantly detected, see Fig. 2), which is compatible with upper limits obtained previously by Xing & Wang (2013) in a search of gamma-ray counterpart of several AMSPs, including SAX J1808.4−3658. If we compare with the total rotational power at present [$\dot{E} = (1.1 \pm 0.2) \times 10^{34}\,\mathrm{erg\,s^{-1}}$ obtained from the values of ν and $\dot{\nu}$ quoted in Table 1 and using a moment of inertia of $10^{45}\,\mathrm{g\,cm^{-2}}$] assuming a beaming factor of $f_\Omega = 1$ (Watters et al. 2009), we obtain an efficiency of $\eta = L_\gamma/\dot{E} \times 100 = (27 \pm 9)$ per cent, which is within the range of efficiencies observed from MSPs detected at high energy (Guillemot 2009; Espinoza et al. 2013; Ray et al. 2013; Abdo et al. 2013). If the association can finally be proven, SAX J1808.4−3658 in X-ray quiescence will be similar to PSR J1311−3430 (Pletsch et al. 2012; Ray et al. 2013), a fast MSP (≈2.5 ms) in a compact binary system (≈2 h). The spectral parameters are also compatible within the current statistics to the ones found for other MSPs with a hard spectrum and a turnover at a few gigaelectronvolts (Espinoza et al. 2013; Abdo et al. 2013).

Two MSPs, PSR J1023+0038 and XSS J12270−4859, have recently been observed to switch between a rotation-powered radio pulsar state and an intermediate state characterized by the presence of an outer accretion disc. In the disc state, these two sources showed a 0.1–100 GeV gamma-ray luminosity of a few $\times\ 10^{34}\,\mathrm{erg\,s^{-1}}$ (de Martino et al. 2010; Hill et al. 2011; Stappers et al. 2014), larger by up to an order of magnitude than the gamma-ray luminosity shown in the radio pulsar state. The brighter gamma-ray output observed from MSPs in the intermediate disc state has been interpreted in terms of an intra-binary shock close to the pulsar (Stappers et al. 2014; Coti Zelati et al. 2014), inverse Compton scattering of UV disc photons by the pulsar wind (Takata et al. 2014; Li et al. 2014), and synchrotron self-Compton emission from the inner disc boundary around a propelling NS (Papitto, Torres & Li 2014b). On the other hand, the lower luminosity observed from the proposed counterpart of SAX J1808.4−3658 is similar to that usually observed from MSPs in the rotation-powered state, and indicates that this is the most likely state in which SAX J1808.4−3658 lies during X-ray quiescence.

A detection of gamma-ray pulsations from SAX J1808.4−3658 would imply rotational-powered activity in quiescence mode, whereas for SAX J1808.4−3658, pulsed emission due to accretion-power mechanisms was detected during the bursting accretion phase. If confirmed, SAX J1808.4−3658 will add to IGR J18245−2452 (Papitto et al. 2013), PSR J1023+0038 (Archibald et al. 2014) and XSS J12270−4859 (Papitto et al. 2014a) as a source showing evidence of a transition to a rotation-powered radio pulsar state in X-ray quiescence, whilst it is observed as an accreting pulsar when it has a disc. That would also emphasize the

potential of the gamma-ray regime for investigating these systems, since it avoids the observational biases suffered in other bands, such as large absorption or narrow radio beams.

4 CONCLUSIONS

In a search for a gamma-ray counterpart for SAX J1808.4−3658, we discovered a weak gamma-ray source when analysing almost 6 yr of data obtained with the LAT experiment. The position of the source is compatible within 3.2 arcmin with the location of SAX J1808.4−3658. The LAT source exhibits an energy flux of $(2.1 \pm 0.5) \times 10^{-12}$ erg cm^{-2} s^{-1} (in the 0.6 to 10 GeV energy range) and a point morphology.

The positional alignment between the gamma-ray source and SAX J1808.4−3658 and the lack of gamma-ray accelerators other than the AMSP suggest an association between the two. However, the uncertainties in the position and rotational ephemeris of SAX J1808.4−3658 prevent a firm identification through phase variability. The uncertainty of the spin and spin frequency derivative will be improved by X-ray studies of the pulsations of the source during its future X-ray outbursts. On the other hand, the positional error is dominated by the 0.15-arcsec uncertainties in the 2MASS catalogue (Skrutskie et al. 2006) used to register the image of the optical counterpart of SAX J1808.4−3658 (Hartman et al. 2008), and will hopefully be improved by future missions devoted to astrometry.

ACKNOWLEDGEMENTS

The work was done under the grants AYA2012-39303, SGR2009-811 and SGR2012-1073. NR acknowledges support from an NWO Vidi Award and NewCOMPSTAR COST Action MP1304. AR acknowledges the Sardinia Regional Government for financial support (P.O.R. Sardegna F.S.E. Operational Programme of the Autonomous Region of Sardinia, European Social Fund 2007–2013, Axis IV Human Resources, Objective I.3, Line of Activity I.3.1). JL and DFT acknowledge support from the National Natural Science Foundation of China via NSFC-11473027. DFT further acknowledges the Chinese Academy of Sciences visiting professorship program 2013T2J0007.

The Fermi LAT Collaboration acknowledges generous ongoing support from a number of agencies and institutes that have supported both the development and the operation of the LAT as well as scientific data analysis. These include the National Aeronautics and Space Administration and the Department of Energy in the United States, the Commissariat à l'Energie Atomique and the Centre National de la Recherche Scientifique/Institut National de Physique Nucléaire et de Physique des Particules in France, the Agenzia Spaziale Italiana and the Istituto Nazionale di Fisica Nucleare in Italy, the Ministry of Education, Culture, Sports, Science and Technology (MEXT), High Energy Accelerator Research Organization (KEK) and Japan Aerospace Exploration Agency (JAXA) in Japan, and the K. A. Wallenberg Foundation, the Swedish Research Council and the Swedish National Space Board in Sweden.

Additional support for science analysis during the operations phase is gratefully acknowledged from the Istituto Nazionale di Astrofisica in Italy and the Centre National d'Études Spatiales in France.

REFERENCES

Abdo A. A. et al., 2009, Astropart. Phys., 32, 193
Abdo A. A. et al., 2013, ApJS, 208, 17
Acero F. et al., 2015, ApJS, 218, 23
Alpar M. A., Cheng A. F., Ruderman M. A., Shaham J., 1982, Nature, 300, 728
Archibald A. M. et al., 2009, Science, 324, 1411
Archibald A. M. et al., 2014, ApJ, 807, 62
Atwood W. B. et al., 2009, ApJ, 697, 1071
Bassa C. G. et al., 2014, MNRAS, 441, 1825
Beckmann V., Soldi S., De Jong S., 2014, in 40th COSPAR Scientific Assembly. Abstract E1.5-16-14, Moscow, Russia, p. 239
Burderi L., Di Salvo T., D'Antona F., Robba N. R., Testa V., 2003, A&A, 404, L43
Burderi L., Riggio A., di Salvo T., Papitto A., Menna M. T., D'Aì A., Iaria R., 2009, A&A, 496, L17
Burgay M., Burderi L., Possenti A., D'Amico N., Manchester R. N., Lyne A. G., Camilo F., Campana S., 2003, ApJ, 589, 902
Caliandro G. A., Torres D. F., Rea N., 2012, MNRAS, 427, 2251
Campana S. et al., 2002, ApJ, 575, L15
Condon J. J., Cotton W. D., Greisen E. W., Yin Q. F., Perley R. A., Taylor G. B., Broderick J. J., 1998, AJ, 115, 1693
Coti Zelati F. et al., 2014, MNRAS, 444, 1783
de Jager O. C., Büsching I., 2010, A&A, 517, L9
de Martino D. et al., 2010, A&A, 515, A25
di Salvo T., Burderi L., Riggio A., Papitto A., Menna M. T., 2008, MNRAS, 389, 1851
Espinoza C. M. et al., 2013, MNRAS, 430, 571
Galloway D. K., Cumming A., 2006, ApJ, 652, 559
Guillemot L., 2009, Ph.D. Thesis, Univ. de Bordeaux
Hartman J. M. et al., 2008, ApJ, 675, 1468
Hartman J. M., Patruno A., Chakrabarty D., Markwardt C. B., Morgan E. H., van der Klis M., Wijnands R., 2009, ApJ, 702, 1673
Heinke C. O., Jonker P. G., Wijnands R., Taam R. E., 2007, ApJ, 660, 1424
Hill A. B. et al., 2011, MNRAS, 415, 235
Homer L., Charles P. A., Chakrabarty D., van Zyl L., 2001, MNRAS, 325, 1471
Iacolina M. N., Burgay M., Burderi L., Possenti A., di Salvo T., 2009, A&A, 497, 445
Iacolina M. N., Burgay M., Burderi L., Possenti A., di Salvo T., 2010, A&A, 519, A13
Kerr M., 2010, PhD thesis, Univ. Washington
Leahy D. A., 1987, A&A, 180, 275
Li K. L., Kong A. K. H., Takata J., Cheng K. S., Tam P. H. T., Hui C. Y., Jin R., 2014, ApJ, 797, 111
Manchester R. N., Peters W. L., 1972, ApJ, 173, 221
Mattox J. R. et al., 1996, ApJ, 461, 396
Papitto A. et al., 2013, Nature, 501, 517
Papitto A., de Martino D., Belloni T. M., Burgay M., Pellizzoni A., Possenti A., Torres D. F., 2014a, MNRAS, 449, L26
Papitto A., Torres D. F., Li J., 2014b, MNRAS, 438, 2105
Papitto A., de Martino D., Belloni T. M., Burgay M., Pellizzoni A., Possenti A., Torres D. F., 2015, MNRAS, 449, L26
Patruno A., Watts A. L., 2012, preprint (arXiv:1206.2727)
Patruno A., Bult P., Gopakumar A., Hartman J. M., Wijnands R., van der Klis M., Chakrabarty D., 2012, ApJ, 746, L27
Patruno A. et al., 2014, ApJ, 781, L3
Pletsch H. J. et al., 2012, Science, 338, 1314
Radhakrishnan V., Srinivasan G., 1982, Current Sci., 51, 1096
Ray P. S. et al., 2013, ApJ, 763, L13
Sanna A. et al., 2015, Astron. Telegram, 7364, 1
Skrutskie M. F. et al., 2006, AJ, 131, 1163
Stappers B. W. et al., 2014, ApJ, 790, 39
Stella L., Campana S., Colpi M., Mereghetti S., Tavani M., 1994, ApJ, 423, L47
Takata J. et al., 2014, ApJ, 785, 131
Watters K. P., Romani R. W., Weltevrede P., Johnston S., 2009, ApJ, 695, 1289
Wijnands R., van der Klis M., 1998, Nature, 394, 344
Xing Y., Wang Z., 2013, ApJ, 769, 119
Xing Y., Wang Z., Jithesh V., 2015, preprint (arXiv:1502.00733)

This paper has been typeset from a TEX/LATEX file prepared by the author.